

## CHAPTER 2 THEORY

### 2.1 Graphite [26]

The word “graphite” is from the Greek word “graphein” which means “to write/draw”, for its use in pencils, where it is commonly called “lead”. In the 15<sup>th</sup> century, the first pencils were produced in England. The color of graphite is black silver as shown in figure 2.1. Its transparency is opaque. It is very hard and brittle.



**Figure 2.1** Graphite specimen [27]

Graphite is an allotrope of carbon. It consists of the stack of parallel layer planes as shown in figure 2.2. In each layer plane, carbon atoms are arranged in a hexagonal lattice. The bond is covalent and has 0.141 nm of a short separation and 524 kJ/mol of high strength. Between layer planes, the bond is van der Waals. It is relatively weak compared to covalent bond and has only 7 kJ/mol of strength. The distance between the layer planes is 0.335 nm which is more than twice the distance between carbon atoms within the basal plane and about twice the van der Waals radius of carbon (170 pm). There are two ways of the stacking of these layer planes. One is hexagonal, the other is rhombohedral.

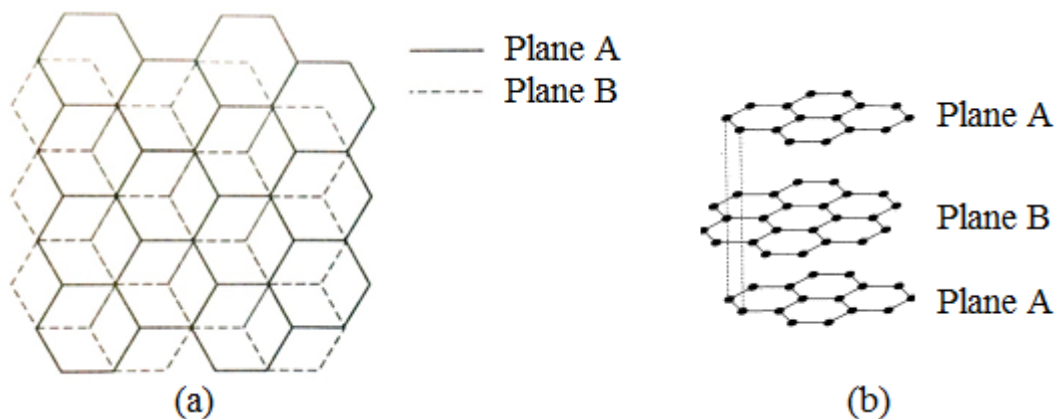


**Figure 2.2** Schematic of hexagonal graphite crystal (a) top view (b) cross section [26]

Hexagonal graphite is the most common stacking sequence of the graphite crystal. Its stacking order is -ABABAB-. Figure 2.2 shows schematic of hexagonal graphite crystal, where the carbon atoms in every other layer are superimposed over each other. Hexagonal graphite is the thermodynamically stable form of graphite and is found in all synthetic materials.

Rhombohedral graphite is shown in figure 2.3. Its stacking order is -ABCABCABC-. The carbon atoms in every third layer are superimposed. It is never found in pure form but always in combination with hexagonal graphite. It can be considered as an extended stacking fault of hexagonal graphite. It is thermodynamically unstable. During heat treatment above 1300°C, it usually reverts to the hexagonal form.

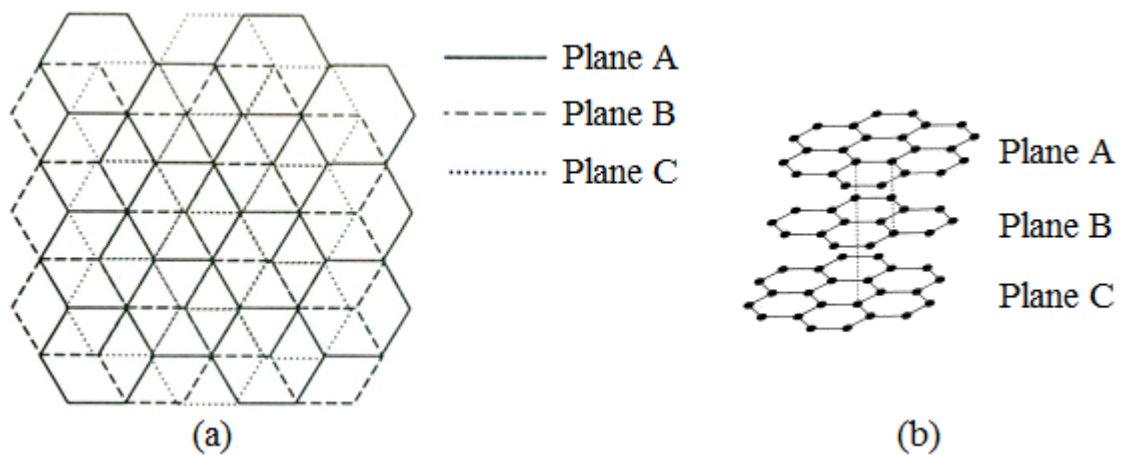


**Figure 2.3** Schematic of rhombohedral graphite crystal (a) top view (b) cross section [26]

**Table 2.1** Physical properties of graphite [26]

<b>Physical properties of graphite</b>	
Crystalline form	Hexagonal
Lattice parameters	$a_0 = 0.246 \text{ nm}$ $b_0 = 0.671 \text{ nm}$
Color	Black silver
Density at 300 K, 1 atm	$2.26 \text{ g/cm}^3$
Atomic volume	$5.315 \text{ cm}^3/\text{mol}$
Sublimation point at 1 atm	4000 K
Triple point	4200 K
Boiling point	4560 K
Heat of fusion	46.84 kJ/mol
Heat of vaporization to monoatomic gas	716.9 kJ/mol
Pauling electronegativity	2.5

The physical properties of graphite are summarized in table 2.1. The density of the perfect crystal is the theoretical value. Most graphite materials will have lower than densities because of the presence of structural imperfections such as porosity, lattice vacancies and dislocations. Graphite does not have a normal melting point since, at one

atmosphere, it does not melt but sublimates when the temperature reaches approximately 4000 K. The triple point is achieved, by recent estimates, at a temperature of 4200 K and a pressure of 1 atm. The heat of vaporization of graphite is high. The large amount of energy required to vaporize graphite is an advantage in the design of ablative structures such as nose cones and rocket nozzles.

Electrically, graphite can be considered as a semi-metal. Its atomic structure is such that the highest-filled valence band overlaps the lowest-empty conduction band by approximately 36 MeV. The delocalized fourth-valence electrons form a partially-filled conduction band between the basal planes where they can move readily in wave pattern as they respond to electric fields. Therefore, the electrical resistivity of graphite parallel to the basal planes (ab directions) is low and the material is considered an electrical conductor. The separation between planes in the c direction is comparatively large. There is no comparable mechanism for the electrons to move from one plane to another. Thus, the electrical resistivity in this direction is high and the material is a relatively electrical insulator.

## 2.2 Nanographite [1, 2, 13]

Nanographite is an allotrope of carbon which is made from graphite. Nanographite consists of a surface inlaid with a graphene sheet of regular hexagons of carbon atoms that remains planar on the micron or sub-micron scale. 10 - 100 nm of graphite thickness is called "nanographite". The bond between layers is van der Waals. Nanographite is of potential technological interest in the realization of high temperature gaskets, as electrodes in lithium recharged batteries, adsorption substrates, or as a reinforcing material in nano-composites, and they can be produced by chemical or mechanical methods. Chemical methods are generally based on the intercalation of graphite followed by rapid thermal annealing. The electronic properties of nanographite change with the number of layers and by the relative position of atoms in adjacent layers (stacking order). As the number of layers increases, the stacking order and the band structure can become more complicated, several charge carriers appear and the conduction and valence bands start notably overlapping. The application of nanographite is versatile, such as super lubricant, energy-storing, high conductor, diamond, etc. For the feature of small and homogeneous particle dimension, it can be used as nanoscaled compound-material or compound-paint additive. For the feature of high-purity and high specific surface area, it is better to be hydrogen storage material than other materials. For the feature of high thermal-stability, electric/anti-corrosion performance and thermal-conduction features, it is a good electric and thermal conductive material.

Li *et al.* [25] showed that the nanographite (DK202) was obtained from Beijing Dk Nano Technology Co., Ltd., China. The particle diameter of the nanographites is 35 nm and the purity is 99.95%. The appearance and microstructure of nanographite is illustrated in figure 2.4. The nanographite is a black powder with a laminar microstructure. The particles pack together loosely.

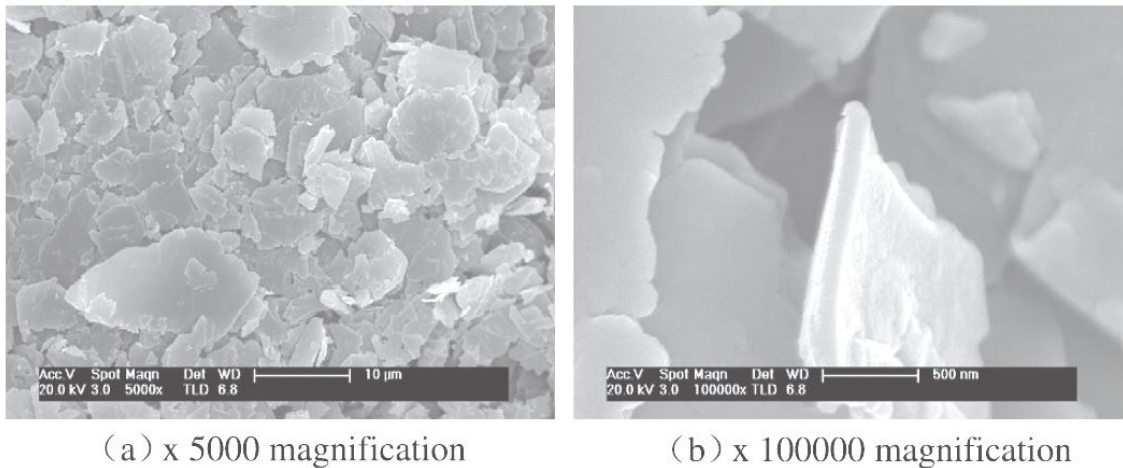


**Figure 2.4** Microstructure of the nanographite: (a)  $\times 5000$  magnification; (b)  $\times 100,000$  magnification [28]

## 2.3 Graphene

Graphene is one of the most interested topics of research since the discovery of material in 2004 by Novoselov, Geim and coworkers [3, 4]. It is an allotrope of carbon. The name of graphene comes from graphite and alkene [29]. It has received significant attention because of its unique physical, optical, mechanical, electrical and thermal properties. It is an ideal material for future nanoelectronics and sensor applications.

### 2.3.1 Morphology and structure of graphene

Graphene is a single layer with a thickness of a single carbon atoms arranged in a two-dimensional hexagonal lattice as shown in figure 2.5. [5]. It is bonded together with  $\sigma$  bond in figure 2.6. Each carbon atom in the lattice has a  $\pi$  orbital that contributes to a delocalized network of electrons. Figure 2.7 shows rippled graphene from a Monte Carlo simulation. It was estimated to have a lateral dimension of approximately 8-10 nm and a height displacement of approximately 0.7-1 nm [9].

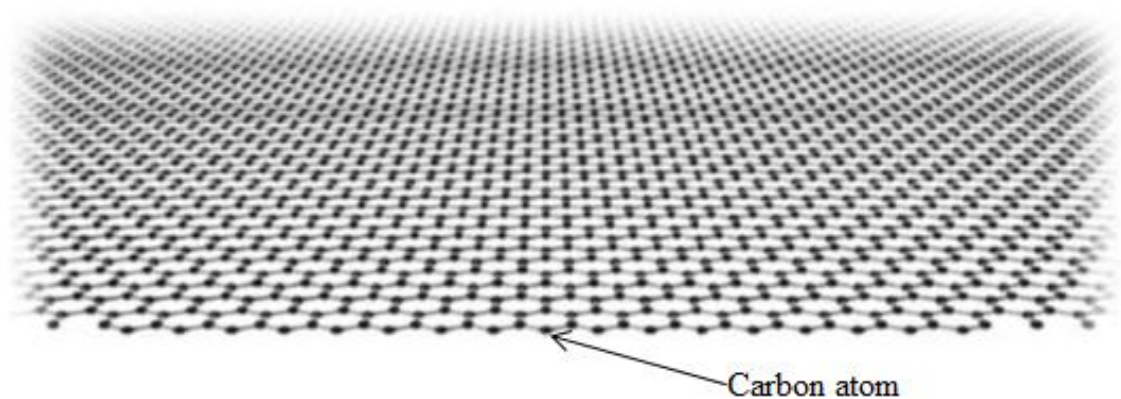


**Figure 2.5** Structure of graphene [30]

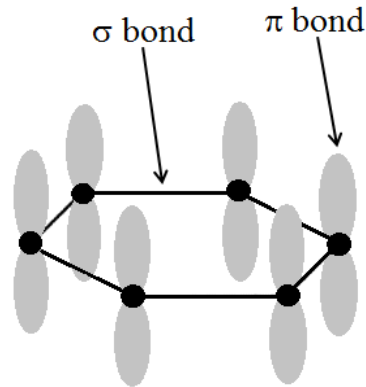


**Figure 2.6**  $\sigma$  and  $\pi$  bond of graphene

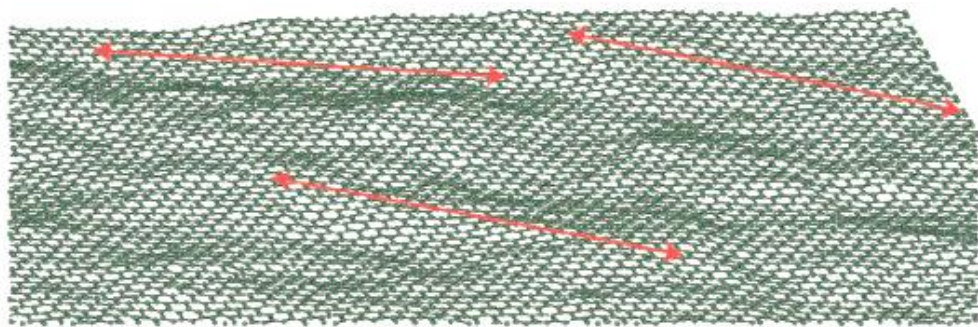


**Figure 2.7** 'Rippled graphene' from a Monte Carlo simulation. The red arrows are  $\sim 8$  nm long [9]

The extension of honeycomb structure is the fundamental building block of other important carbon-based materials. It can be packed into form three dimensional graphite, rolled to form one dimensional nanotubes, and wrapped to form zero dimensional buckyballs as shown in figure 2.8. It also is widely to explain properties of these allotropes [8, 31].

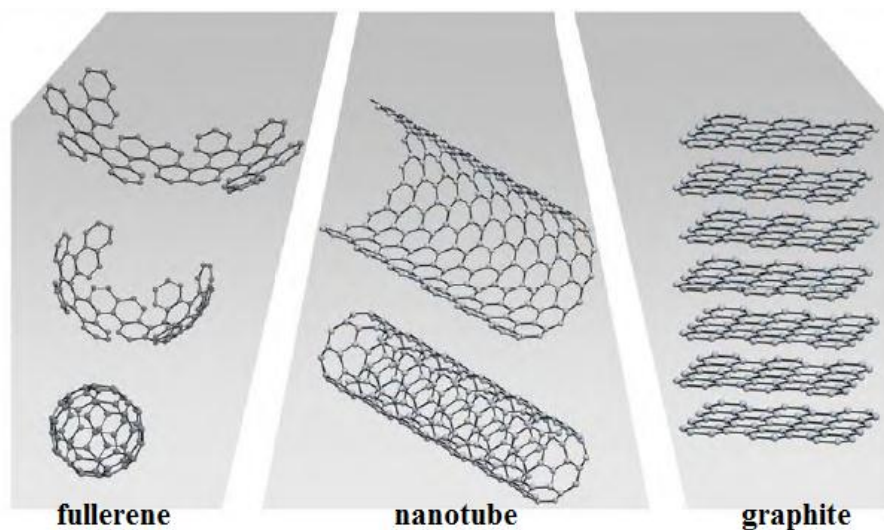


**Figure 2.8** Graphene: mother of all graphitic forms [30]

## 2.3.2 Synthesis of graphene

Many research groups have been fastened to study and synthesize graphene using various techniques which have different advantages and disadvantages.

### 2.3.2.1 Scotch tape method [5]

The isolation of graphene was first introduced by mechanical exfoliation or scotch tape method. A piece of scotch tape is used to peel graphene flakes off of a stack of graphite as shown in figure 2.9. This method exhibit a high quality of graphene, but it cannot offer a large size of graphene and a large scale production.

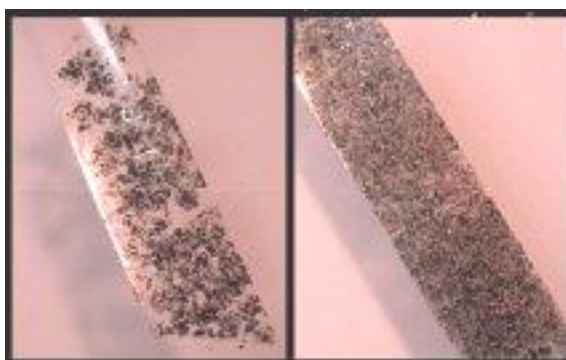


**Figure 2.9** Synthesis of graphene by scotch tape method [5]

### 2.3.2.2 Hummers' method [32]

Hummers' method is one of a low-cost approach. However, this oxidation process causes damage on the honeycomb structure of graphene. Graphite powders were oxidized using three different methods: Hummers' method, improved Hummers' method, and Hummers' method with additional  $\text{KMnO}_4$ .

For Hummers' method, a mixture of graphite flake (3.0 g) and  $\text{NaNO}_3$  (1.5 g) was added  $\text{H}_2\text{SO}_4$  (69 mL), then the mixture was cooled to  $0\text{ }^\circ\text{C}$  using an ice bath.  $\text{KMnO}_4$  (9.0 g) was added slowly in portions to keep the reaction temperature below  $20\text{ }^\circ\text{C}$ . The reaction was warmed to  $35\text{ }^\circ\text{C}$  and stirred for 30 minutes, at which time 138 mL of water was added slowly, producing a large exotherm to  $98\text{ }^\circ\text{C}$ . External heating was introduced to maintain the reaction temperature at  $98\text{ }^\circ\text{C}$  for 15 minutes, then the heat was removed and the reaction was cooled using a water bath for 10 minutes. Additional 420 mL of water and 3 mL of  $\text{H}_2\text{O}_2$  (30%) were added, producing another exotherm. After air cooling, the mixture was purified as described for the individual graphene oxide above (sifting, filtration, multiple washings, centrifugations and decanting, vacuum drying) to give 1.2 g of solid.

For the improved Hummers' method, a mixture of concentrated  $\text{H}_2\text{SO}_4$  (360 mL) and  $\text{H}_3\text{PO}_4$  (40 mL) was added to a mixture of graphite flakes (3.0 g) and  $\text{KMnO}_4$  (18.0 g), producing a slight exotherm to  $35\text{-}40\text{ }^\circ\text{C}$ . The reaction was then heated to  $50\text{ }^\circ\text{C}$  and stirred for 12 h. The reaction was cooled to room temperature and poured onto ice (~

400 mL) with 3 mL of H<sub>2</sub>O<sub>2</sub> (30%). For workup, the mixture was sifted through a metal U.S. Standard testing sieve (W.S. Tyler, 300 μm) and then filtered through polyester fiber (Carpenter Co.) The filtrate was centrifuged at 4000 rpm for 4 h, and the supernatant was decanted away. The remaining solid material was then washed in succession with water (200 mL), 30% HCl (200 mL), and ethanol (200 mL); for each wash, the mixture was sifted through the U.S. Standard testing sieve and then filtered through polyester fiber with the filtrate being centrifuged at 4000 rpm for 4 h and the supernatant decanted away. The material remaining after this extended, multiple-wash process was coagulated with ether (200 mL) and the resulting suspension was filtered over a PTFE membrane with a 0.45 μm pore size. The solid obtained on the filter was vacuum-dried overnight at room temperature, obtaining 5.8 g of product.

For Hummers' method with additional KMnO<sub>4</sub>, concentrated 69 mL of H<sub>2</sub>SO<sub>4</sub> was added to a mixture of graphite flakes (3.0 g) and NaNO<sub>3</sub> (1.5 g), and the mixture was cooled using an ice bath to 0 °C. 9.0 g of KMnO<sub>4</sub> was added slowly in portions to keep the reaction temperature below 20 °C. The reaction was warmed to 35 °C and stirred for 7 h. Additional KMnO<sub>4</sub> (9.0 g) was added in one portion, and the reaction was stirred at 35 °C for 12 h. The reaction mixture was cooled to room temperature and poured onto ice (~ 400 mL) with 30% H<sub>2</sub>O<sub>2</sub> (3 mL). The mixture was then purified following the previous protocol of sifting, filtering, centrifugation, decanting with multiple washes followed by a final vacuum drying to give 4.2 g of solid product.

ACS material enterprise [33] showed TEM image of graphene oxide which obtained from Hummers' method as shown in figure 2.10. This TEM analysis was completed through dispersing graphene oxide into water or ethanol with the help of ultrasound. Thickness of this graphene oxide is about 0.8-1.2 nm. The particle diameter of this graphene oxide is about 1-5 μm and the purity is about 99%.

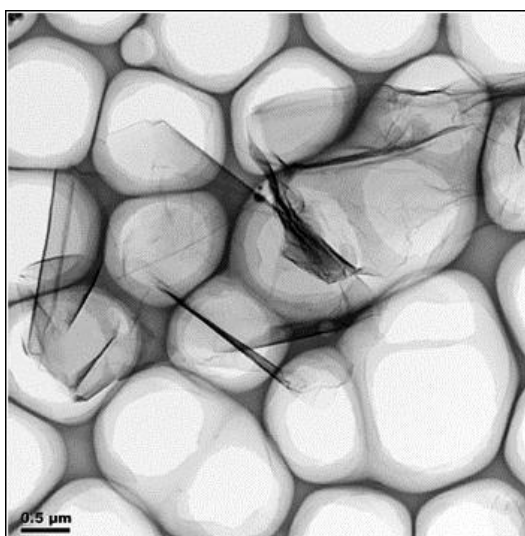


**Figure 2.10** TEM image of graphene oxide which obtained from Hummers' method [33]

### 2.3.2.3 Chemical vapor deposition (CVD) [34]

Chemical vapor deposition (CVD) methods have shown to be another suitable technique for achieving a large scale production of graphene, but the process requires high temperature ( $\sim 1,000$  °C) for operating and costs a lot of money. Many researchers have putted many efforts on such achievement; however, it seems that achieving of a large scale production with less graphene damaging is still a bottleneck.

Initially, substrate was prepared for use in a CVD method. Metal was deposited via evaporation process onto substrate. In the experiment of Matthew O' Brien and Barbara Nichols, nickel was deposited via electron beam evaporation onto silicon sunstrate with  $1\ \mu\text{m}$  thermal silicon dioxide ( $\text{SiO}_2$ ) as shown in figure 2.11(a). Figure 2.11(b) showed graphene growth which was achieved by the flow of methane and hydrogen gasses over a nickel thin film acting as catalyst at ambient pressure using CVD process.

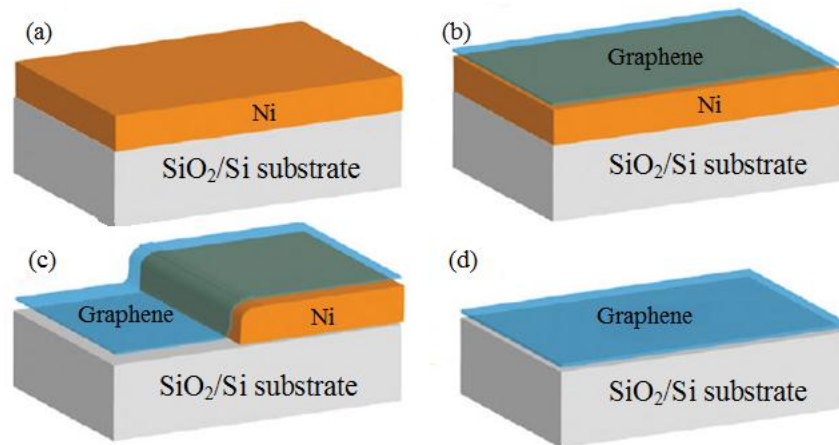


**Figure 2.11** Graphene synthesis by CVD (a) nickel was deposited via electron beam evaporation on a  $\text{SiO}_2/\text{Si}$  substrate (b) then used CVD to lay down a graphene film over the nickel. (c) The nickel evaporates leaving (d) the graphene film directly on the  $\text{SiO}_2/\text{Si}$  substrate [34]

The synthesis process of graphene via CVD is shown in figure 2.12. It begins with heating the substrate to the desired furnace setpoint temperature in an argon and hydrogen atmosphere. Once this temperature was obtained, a 20 minutes annealing step was conducted, allowing temperature stabilization and nickel grain growth. At the end of this period, growth was started by introducing methane, which acts as the carbon source. Duration of this “growth” phase was 10 minutes, and the end was signaled by reducing the heat source at the appropriate cooling rate and allowing the furnace to return to room temperature. With the greatest temperature decrease occurring immediately following the end of the “growth” stage, we focused on control of this temperature region ( $900\text{--}1000$  °C to  $500\text{--}600$  °C). Cooling rates were measured in the first five to ten minutes with an in-tube thermocouple and altered from the natural furnace cooling rate ( $\sim 25$  °C/min) by programming a furnace ramp down rate (e.g., 5 or 10 °C/min). Once the tube temperature reached 500 °C, methane and hydrogen flows were stopped in favor of argon, with little presumed precipitation or growth occurring

below this temperature. The nickel was evaporated leaving (figure 2.11(c)). Figure 2.11(d) showed graphene film directly on the SiO<sub>2</sub>/Si substrate.

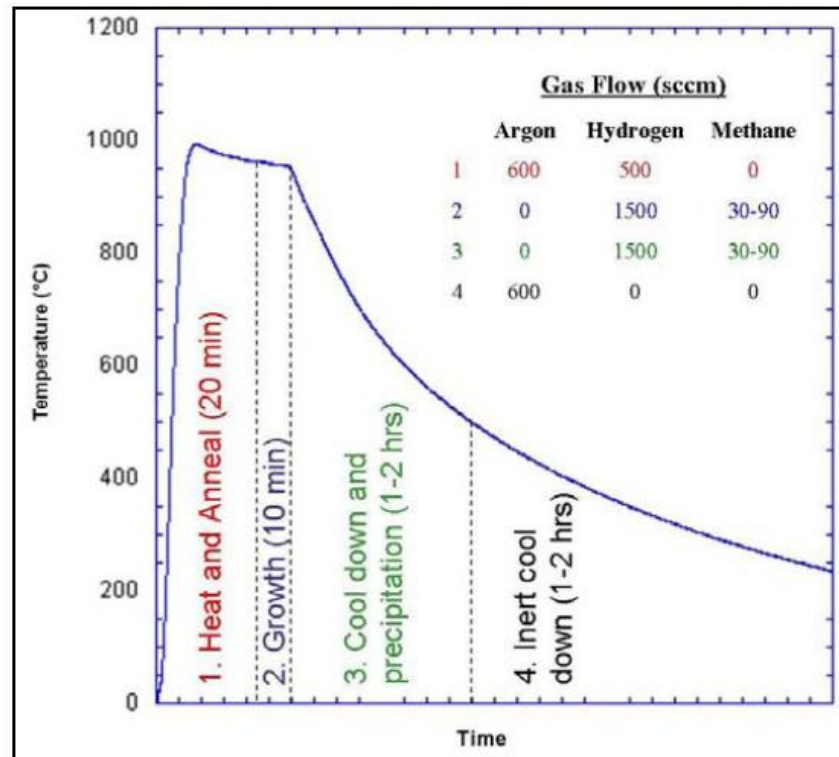


**Figure 2.12** Reaction timeline detailing the CVD process for graphene and its different stages [34]

#### 2.3.2.4 Electrochemical exfoliation [7]

For electrochemical exfoliation, source of graphene is natural graphite flake which was adhered to a tungsten wire by silver pad and employed as an electrode. The graphite flake was inserted as anode into the ionic solution. A grounded platinum wire was placed parallel to the graphite flake with a separation of 5 cm as shown in figure 2.13(a). The ionic solution was prepared by dilution of sulfuric acid (4.8 g) in 100 mL of DI water. The electrochemical exfoliation process was carried out by applying DC bias on graphite electrode from -10 to +10 V. To prepare the graphene sheet suspension, the exfoliated graphene sheets were collected with a 100 nm porous filter and washed with DI water by vacuum filtration. After drying, they were dispersed in DMF solution by gentle water-bath sonication for 5 minutes. To remove unwanted large graphite particles produced in the exfoliation, the suspension was subjected to centrifugation at 2500 rpm. The centrifuged suspension can then be used for further characterizations and film preparation. All of these electrochemical exfoliation experiments were performed at room temperature ( $25 \pm 3$  °C).

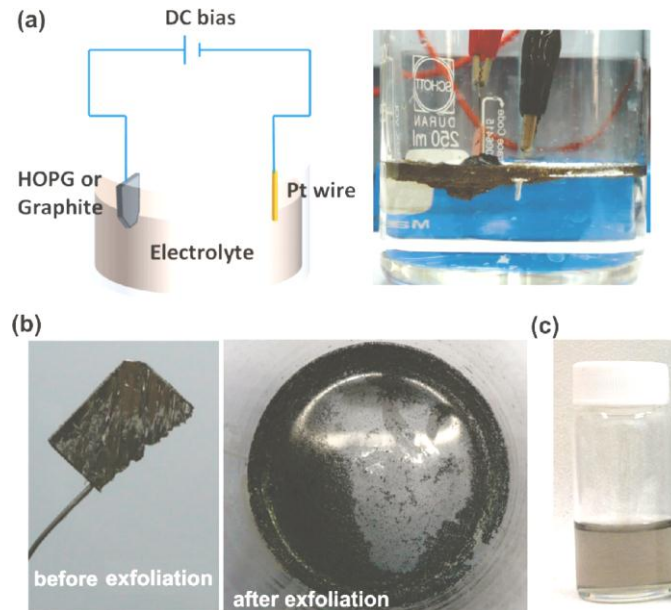


**Figure 2.13** (a) Schematic illustration and photo for electrochemical exfoliation of graphite. (b) Photos of the graphite flakes before and after electrochemical exfoliation. (c) Photo of the dispersed graphene sheets in a DMF solution [7]

### 2.3.2.5 Sonication technique [5]

Graphene can be exfoliated from graphite using sonication method, where it is commonly called “ultrasonic treatment”. Ultrasonic bath uses high frequency sound waves ( $\geq 20$  kHz) to agitate in a liquid. As shown in figure 2.14, cavitation bubbles are induced by the agitation. These bubbles act on graphite. This action also penetrates graphite which can reduce the strengths of van der Waals dispersion forces. Moreover, sonication can generate vibrational force which can break van der Waals dispersion forces. Sonication has a positive effect on graphene exfoliation. It is an easy method with a simple preparation and low cost. However, it may decrease the planar size of the graphene. Si *et al.* [5] prepared graphite oxide by oxidizing graphite flakes with acid, and, then, graphite oxide was sonicated to yield graphene oxide. Therefore, sonication has positive effect on material exfoliation.

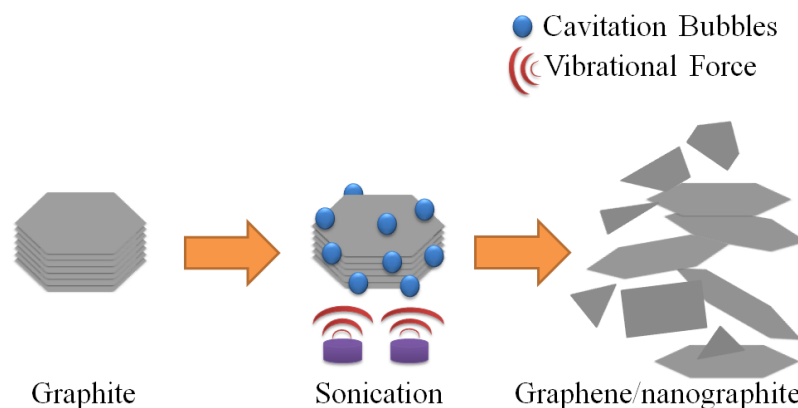


**Figure 2.14** Schematic of sonication for graphene/nanographite synthesis

### 2.3.3 Property of graphene [9, 35]

Graphene is distinctly different from carbon nanotubes and buckyballs. It exhibits many unique physical, optical, mechanical, electrical and thermal properties which have fascinated the scientific community. It is a two dimensional material which is constructed with a monolayer of carbon atoms forming hexagonal rings.

Graphene is the thinnest material in our universe. As shown in figure 2.15(a), graphene is a high transparency material. Its optical transmittance is about 97.7%. This transparency has been experimentally observed in the visible range. The transmittance linearly decreases with the number of layers for n-layer graphene as shown in figure 2.15(b) which shows optical image of graphene flakes with one, two, three and four layers on a 285 nm thick SiO<sub>2</sub> on Si substrate. This optical property is useful to develop transparent electrode and coating applications. Theoretically, graphene has high surface area which is about 2630 m<sup>2</sup>/g for a single layer graphene.

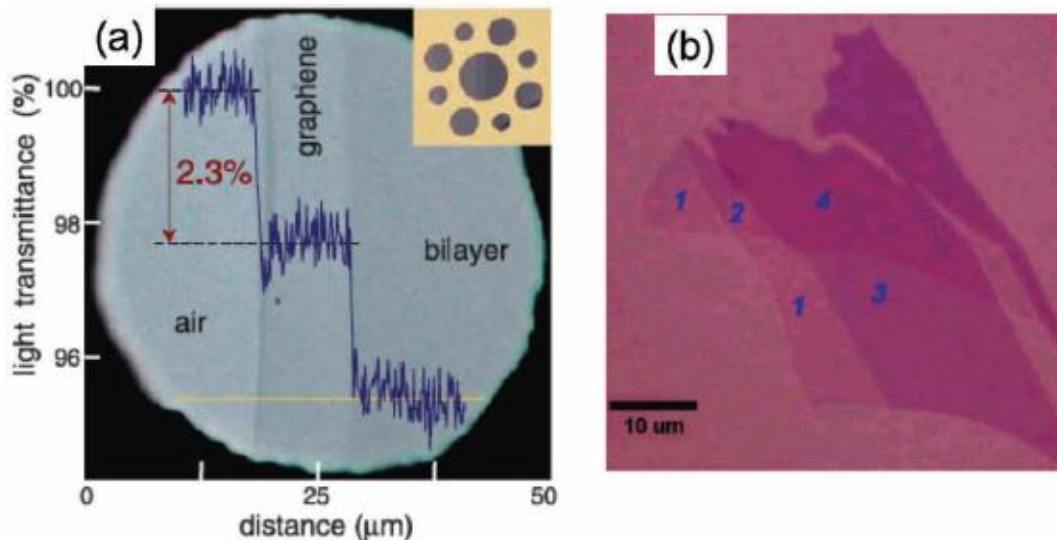


**Figure 2.15** (a) Photograph of a 50  $\mu\text{m}$  aperture partially covered by graphene and its bilayer. The line scan profile shows the intensity of transmitted white light along the yellow line. Inset shows the sample design: a 20  $\mu\text{m}$  thick metal support structure has apertures 20, 30, and 50  $\mu\text{m}$  in diameter with graphene flakes deposited over them; (b) Optical image of graphene flakes with one, two, three, and four layers on a 285 nm thick SiO<sub>2</sub>-on-Si substrate [9]

The mechanical properties of single layer graphene include Young's modulus and mechanical strength. They have been explained by numerical simulations such as molecular dynamics. Experimentally, the Young's modulus of few layer graphene was tested with force-displacement measurements using atomic force microscopy (AFM) on a strip of graphene suspended over trenches. Circular membranes of few layer graphene were also characterized with force-volume measurements by AFM. Recently, the flexibility properties and intrinsic breaking strength of free-standing single layer graphene were measured by nanoindentation using AFM as shown in figure 2.16(a) and

(b). It was reported that defect-free graphene has high elasticity. Its Young's modulus is measured to be about 1 TPa. The mechanical strength of graphene is excellent due to its orderly arrangement of carbon atoms. Moreover, the hexagonal structure of graphene is similar to net. Therefore, the distribution force of graphene is excellent.

High mechanical strength and flexibility of graphene may lead to further development on flexible solar cell which is not easy to crack and non-grain boundary.

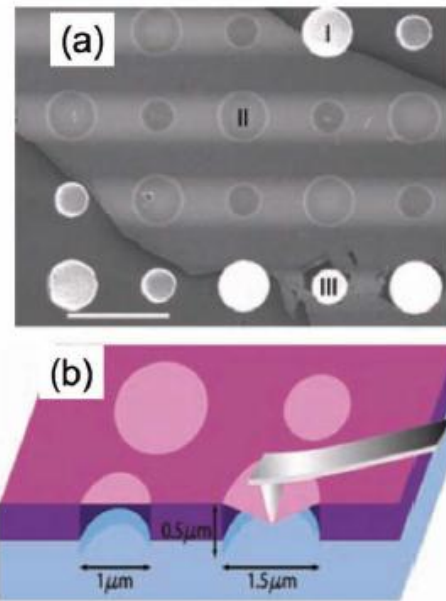


**Figure 2.16** (a) Scanning electron microscopy (SEM) image of a graphene flake spanning an array of circular holes (scale bar, 3 μm) and (b) Schematic illustration of nanoindentation on membranes [9]

Recently, many research groups focus their works on the unusual electron transport properties of graphene which suits for electrode fabrication. Theoretically, graphene is the most stable electrical conducting material because its periodic structure of carbon atoms is arranged in an orderly repeating pattern of two-dimension and non-defect, thus electrons can travel very long distances without scattering in graphene plane. Experimental observation of the cyclotron mass dependence on the square root of the electronic density in graphene was interpreted as evidence for the existence of massless Dirac quasiparticles in graphene. As a zero band gap semiconductor, graphene displays an ambipolar electric field effect and charge carriers can be tuned continuously between electrons and holes in concentrations as high as  $10^{13} \text{ cm}^{-2}$ , with room temperature mobilities of up to  $15,000 \text{ cm}^2/\text{V}\cdot\text{s}$ . Moreover, the observed mobilities depend weakly on temperature, suggesting that an ultrahigh mobility could be realized in graphene at room temperature. Graphene has high intrinsic carrier mobility which is about  $200,000 \text{ cm}^2/\text{V}\cdot\text{s}$  by minimizing impurity scattering. Electron mobility in graphene also is 10 times higher than in commercial grade silicon. The mobility in graphene remains high even at high carrier density in both electrically and chemically doped devices, displaying evidence of ballistic transport on the sub-micrometer scale.

Graphene has superior thermal conductivity which is about 5000 W/m·K. Its thermal conductivity is dominated by phonon transport, namely diffusive conduction at high temperature and ballistic conduction at sufficiently low temperature. It also has high capacity.

### **2.3.4 Application of graphene [14]**

Graphene has outstanding properties which will lead to an application in many technology areas.

#### **2.3.4.1 Microchip**

Graphene can be used to make ultra-fast microchip which was developed by researchers at MIT. It can operate at 1,000 GHz which is much higher speed than silicon chip because of the higher speed at which electrons in graphene move compared to electrons in silicon. These high speed microchips can improve the rate of data transfer for electronic device.

#### **2.3.4.2 Transistor**

Graphene can replace silicon transistors. Graphene-based transistor is more excellent than silicon one. It can run at high frequency. It is much more efficient. These superior graphene-based transistors can increase the speed and capacity of computing.

#### **2.3.4.3 Ultracapacitor**

Graphene may lead to further development on an ultracapacitor. Graphene-based ultracapacitor is light, flexible and easy to maintain. It can store more energy than current batteries because graphene-based ultracapacitors store electrons on graphene sheets, taking advantage of the large surface of graphene to provide increase the electrical power that can be stored in the capacitor. Its efficiency is high. It also has a longer life.

#### **2.3.4.4 Sensor**

The development of graphene-based sensor has received attention. It can be used as ultra-sensitive and ultra-fast electronic sensor. It is able to detect atom or molecule of such gases and chemicals because of its sensitive structure. In addition, graphene has low electrical noise. These graphene-based electronic devices have received significant regard.

#### **2.3.4.5 Solar cell**

Graphene thin films can be used to make electrodes because of its two chief properties, its electrical conductivity and optical transparency. Researchers have found that graphene can replace conductive indium tin oxide (ITO) electrodes in organic solar cells. ITO is expensive and fragile. Graphene can show a high electrical conductivity

and is also stronger and much more flexible than indium tin oxide, and thus could even be used for foldable displays and thin solar cells.

#### 2.3.4.6 Enhanced plastic

Graphene can be mixed with plastic products such as aircraft parts, car parts, sports and household goods. Graphene-plastic composites could be used to replace metals. By doing this, plastics could be made stronger, lighter and more environmentally friendly than pure plastic product.

#### 2.3.4.7 Next generation display

Graphene can replace indium-based electrodes in organic light emitting diodes (OLEDs). Researchers have successfully developed OLEDs with a few nanometer of graphene as transparent conductor. These diodes are used in electronic device display screens which require low power consumption. The use of graphene instead of indium can reduce the cost and eliminates the use of metals in the OLED, which may make devices easier to recycle.

### 2.4 Chemical sensor [17, 18]

Sensor is easily understood. We may imagine a sensor similar to a sensing organ or a tentacle of an ant. A generation ago, the word sensor was not widely used. Today, however, sensors are becoming widespread in our daily lives. Our world is changing rapidly, and sensors play an important role in this process. Sensor started to gain currency during the 1970s. A sensor is commonly called “detector”. Figure 2.17 shows diagram of basic sensor operations. Sensor is a device that measures a physical quantity and converts it into a signal. That signal is read by an observer or instrument. Physical quantities are temperature, light, sound, mechanical force, atmospheric pressure, displacement, velocity, acceleration and flow. The main component of sensor measurement system is shown in figure 2.18.



Figure 2.17 Diagram of basic sensor operations [17]

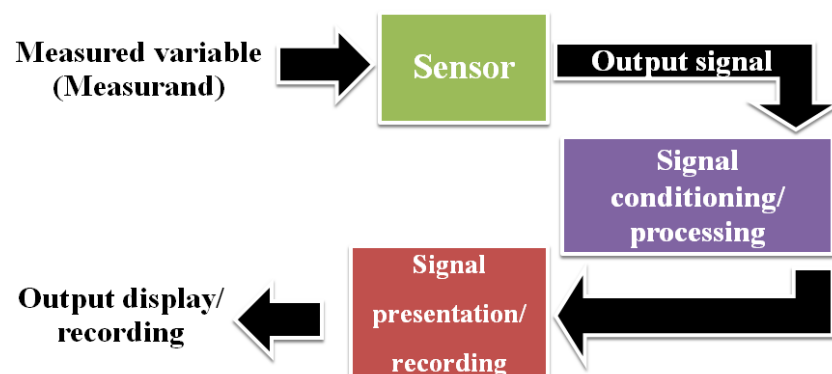
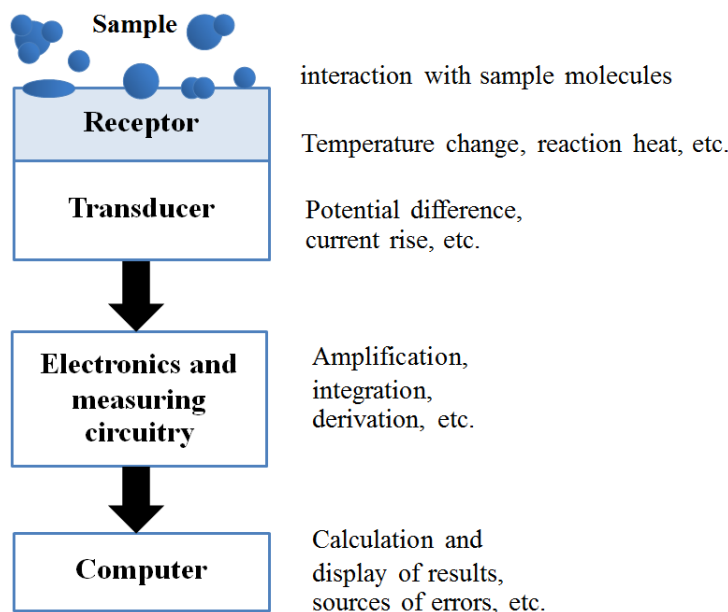


Figure 2.18 The main component of sensor measurement system [17]

Chemical sensor is a special variety of sensors. It is a device that transforms chemical information, ranging from concentration of a specific sample component to total composition analysis, into an analytically useful signal. Chemical sensors have found a wide range of applications in clinical, industrial, environmental, agricultural, and military technologies. They are characterized by parameters such as sensitivity, selectivity, response and recovery time, and saturation. Figure 2.19 shows the functions of a chemical sensor. It usually contains two basic components connected in series: a chemical (molecule) recognition system (receptor) and a physicochemical transducer.



**Figure 2.19** Scheme of a typical chemical sensor system [17]

The mechanism of chemical sensors, the receptor interacts with analyte molecules. Its physical properties are changed in such a way that the appending transducers can gain an electrical signal. For instant in metallic oxide semiconductor gas sensors which change their electrical conductivity in contact with some gases. Conductivity change itself is a measurable electrical signal.

Table 2.2 shows the parameters which can be used to characterize the performance of chemical sensors.

**Table 2.2** Parameters of chemical sensors [17]

<b>Parameters of chemical sensors</b>	
Sensitivity	Change in the measurement signal per concentration unit of the analyte, i.e. the slope of a calibration graph
Detection limit	The lowest concentration value which can be detected by the sensor in question, under definite conditions. Whether or not the analyte can be quantified at the detection limit is not determined. Procedures for evaluation of the detection limit depend on the kind of sensor considered.
Dynamic range	The concentration range between the detection limit and the upper limiting concentration.

**Table 2.2** Parameters of chemical sensors (cont'd)

<b>Parameters of chemical sensors</b>	
Selectivity	An expression of whether a sensor responds selectively to a group of analytes or even specifically to a single analyte. Quantitative expressions of selectivity exist for different types of sensors. For potentiometric sensors, it is given by the selectivity coefficient.
Linearity	The relative deviation of an experimentally determined calibration graph from an ideal straight line. Usually values for linearity are specified for a definite concentration range.
Resolution	The lowest concentration difference which can be distinguished when the composition is varied continuously. This parameter is important chiefly for detectors in flowing streams.
Response time	The time for a sensor to respond from zero concentration to a step change in concentration. Usually specified as the time to rise to a definite ratio of the final value. Thus, e.g. the value of $t_{99}$ represents the time necessary to reach 99 percent of the full-scale output. The time which has elapsed until 63 percent of the final value is reached is called the time constant.
Hysteresis	The maximum difference in output when the value is approached with (a) an increasing and (b) a decreasing analyte concentration range. It is given as a percentage of full-scale output.
Stability	The ability of the sensor to maintain its performance for a certain period of time. As a measure of stability, drift value are used, e.g. the signal variation for zero concentration.
Life cycle	The length of time over which the sensor will operate. The maximum storage time (shelf life) must be distinguished from the maximum operating life. The latter can be specified either for continuous operation or for repeated on-off cycles.

## 2.5 pH sensor [19]

An intrinsic value of all aqueous solutions is the pH value. There is a pH value in each aqueous solution. pH is one of the most often calculated and measured properties of solutions, products and substances. At 25°C pure water, amount of H<sup>+</sup> and OH<sup>-</sup> ions is equal. This state is called neutral with a pH value of 7. The pH scale covers values between 0 and 14. Acids have pH values towards 0. Base solutions have pH values towards 14. The pH value is important in almost any area concerned with water. For example, pH value measuring is also important for agriculture and environment such as pH testing in shrimp pond, acid or base testing in yogurt, curd and salted soya beans factory. Drinking water of the European demands a pH value of 6.5–9.5. Water with pH lower 6.5 can cause corrosion of metal pipes and give rise to high concentrations of heavy metal ions in drinking water. For swimming pools hygiene and health are the main reason for restricting the pH value to 6.8–7.6. Too high values affect the

disinfection process, and too low values may lead to skin irritation. To monitor these pH value, we need an effective sensor which is able to detect pH value.

pH sensor is an electronic device used for measuring the pH (acid or base) of a liquid. It is one type of chemical sensor. Basic pH sensor operations, the main component of pH sensor measurement system and typical pH sensor system is similar to chemical sensor in topic 2.4. A typical pH sensor consists of a special measuring probe connected to an electrode that measures and displays the pH reading. The operation of pH sensor is similar to typical electronic devices. Just only soaking of pH sensor probe into solution is easy to read pH value. pH sensor transforms chemical information, ranging from concentration of a specific sample component to total composition analysis, into an analytically useful signal.

## 2.6 Ultrasonic bath [39]

An ultrasonic bath is a device for cleaning as shown in figure 2.20. It uses ultrasound and an appropriate cleaning solvent to clean delicate items. It is used to clean many types of objects like jewelry, lenses, science glassware, and electronic equipment, etc. Ultrasonic bath is the application of ultrasound. Ultrasound is a cyclic sound pressure wave with a frequency greater than the upper limit of the human hearing range. Ultrasound can be used for imaging, detection, measurement, and cleaning. In ultrasonic bath, an ultrasound built into the chamber produces ultrasonic waves in the liquid using piezo-electric transducer which is a device that converts electrical energy to mechanical one. High frequency sound waves are generated to agitate in a liquid. Cavitation bubbles are induced by the agitation. These bubbles act on contaminants adhering to substrates like metals, plastics, glass, rubber, and ceramics. This action also passes through blind holes and cracks.



**Figure 2.20** Ultrasonic bath [40]

Ultrasonic bath can use for sonication which is commonly called “ultrasonic treatment”. It is the act of applying high frequency sound waves to agitate particles in a liquid for various purposes. In the laboratory, it is usually applied using an ultrasonic bath, colloquially known as a sonicator. Sonication has various effects both chemical and

physical. The chemical effects of ultrasound are concerned with understanding the effect of sonic waves on chemical systems. The chemical effects of ultrasound do not come from a direct interaction with molecular species.

## 2.7 Scanning electron microscopy (SEM) [41-44]



**Figure 2.21** Scanning electron microscopy [45]

The scanning electron microscope is powerful instrument which permit the observation and characterization of heterogeneous organic and inorganic materials and surfaces on such a local scale. It is used for observe, analyze, and correctly explain phenomena on micrometer or submicrometer scale. It can image and analyze bulk specimens. The area to be examined, or the microvolume to be analyzed, is irradiated with a finely focused electron beam, which may be static or swept in a raster across the surface of the specimen. The signals of greatest interest in the scanning electron microscope are the secondary and backscattered electrons because these electrons vary as a result of differences in surface topography as the electron beam is swept across the specimen. The secondary electron emission is confined to a volume near the beam impact area, permitting images to be obtained at relatively high resolution. The three dimensional appearance of the images is due to the large depth of field of the scanning electron microscope as well as to the shadow relief effect of the secondary electron contrast.

In figure 2.22, modern SEMs are controlled by a PC. A, anode; BSE, backscattered electrons; C, cathode; ConA, condenser aperture; ConL, condenser lens; CL, cathodoluminescence; Defl. X, pair of beam deflection coils in the X direction; Defl. Y, pair of beam deflection coils in the Y direction; Det., detectors; DF-D, dark-field detector; O, specimen; OA, objective aperture; OL, objective lens; PC, personal computer; SE, secondary electrons; STEM, scanning transmission electron microscope signal; W, Wehnelt cylinder; X-ray, X-ray signal.

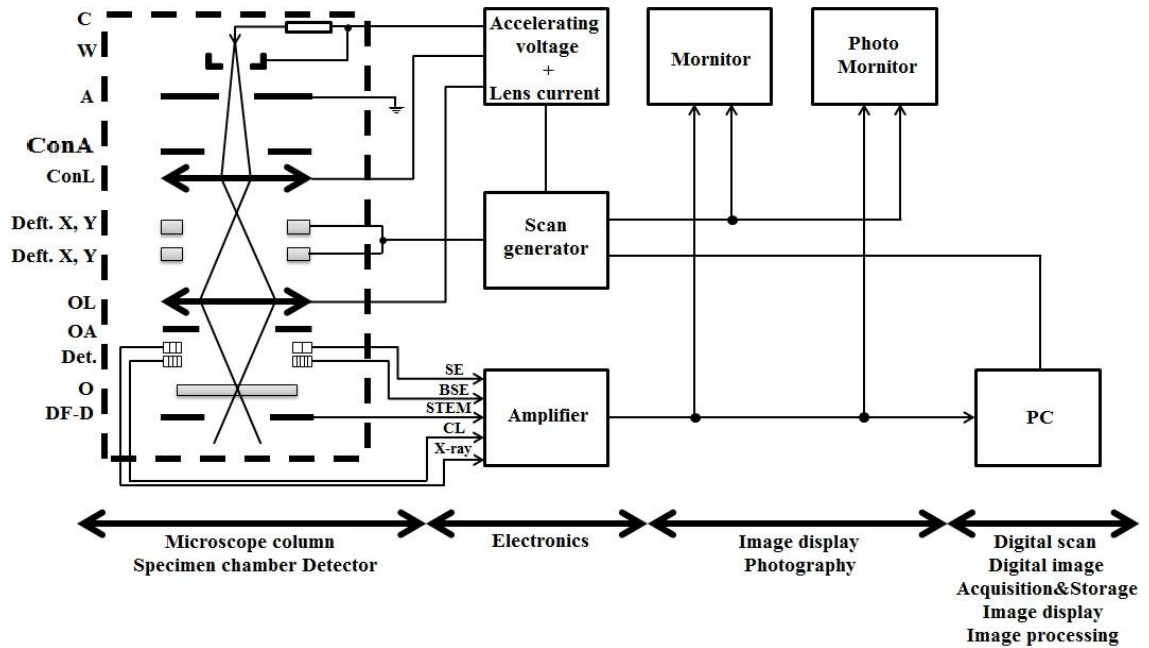


**Figure 2.22** Schematic drawing of a conventional SEM. The evacuated microscope column (inside the bold dashed frame) contains the electron gun, electromagnetic lenses, electromagnetic deflection coils, apertures, the specimen stage, and the detectors. The electronics console houses the power supplies for the acceleration voltage and the electromagnetic lenses, the scan generator, amplifiers for the signals, and monitors for display and recording of images [43]

The principle of the scanning electron microscope is shown in figure 2.22. The two major parts are the microscope column and the electronic console. The microscope column consists of the electron gun (with the components cathode, Wehnelt cylinder, anode), one or two condenser lenses, two pairs of beam deflection coils (scan coils for X, Y deflection), the objective lens, and some apertures. In the specimen chamber at the lower end of the microscope column are located the specimen stage and the detectors for the different signals generated by the electron-specimen interaction. The microscope column and the specimen chamber are evacuated using a combination of prevacuum and high vacuum pumps (usually oil diffusion pumps). The pressure in the specimen chamber typically amounts to about  $10^{-4}$  Pa, allowing the beam electrons to travel from the cathode to the specimen with little interaction with the residual gas molecules. The electronics console consists of the electric power supplies for the acceleration voltage (usual range about 0.5-30 kV) as well as the condenser and objective lenses, the scan generator, and electronic amplifiers for the different signals acquired. Moreover, the console also houses one or more monitors [cathode ray tube (CRT) or liquid crystal displays (LCD)] for displaying the micrographs, a photo-CRT for analogous image recording, and numerous knobs and a computer keyboard to control the electron beam, the signals selected, and the image recording. Now modern SEMs mostly use PC to control the electron beam, to select the signals, and to record as well as to store the

digital images. In that case the numerous knobs are obsolete and are replaced by a mouse-controlled interactive program running on the PC.

The beam electrons are emitted from the cathode and accelerated by a voltage of 0.5-30 kV between the cathode and anode forming a smallest beam cross section-the crossover-near the anode with a diameter of about 10-50  $\mu\text{m}$ . This spot size is too large to produce a sharp image. Therefore the crossover is demagnified by the lens system consisting of one or two condenser lenses and one objective lens and focused on the specimen surface. Most SEMs can produce an electron beam having a smallest spot size of about 5-10 nm and an electron probe current in the range of  $10^{-12}$ - $10^{-10}$  A, which is sufficient to form an image with a reasonable signal-to-noise (S/N) ratio. For higher probe currents required for some modes of operation the smallest probe spot size increases to 100 nm or more. The objective lens has a variable relatively long focal length that allows a large working distance (WD; it corresponds to the distance between the specimen and lower pole piece) in the range of about 5-30 mm. This ensures that the various signals generated by the impinging beam electrons (figure 2.23) in the small specimen interaction volume can be collected by detectors located lateral above the specimen with sufficient efficiency. Pairs of beam deflection coils located in front of the objective lens and controlled by a scan generator scan the electron probe line by line across a small area of the specimen. Simultaneously, the scan generator controls the deflection coil system of a monitor. The intensity of the monitor is modulated by the amplified signal selected by the operator.

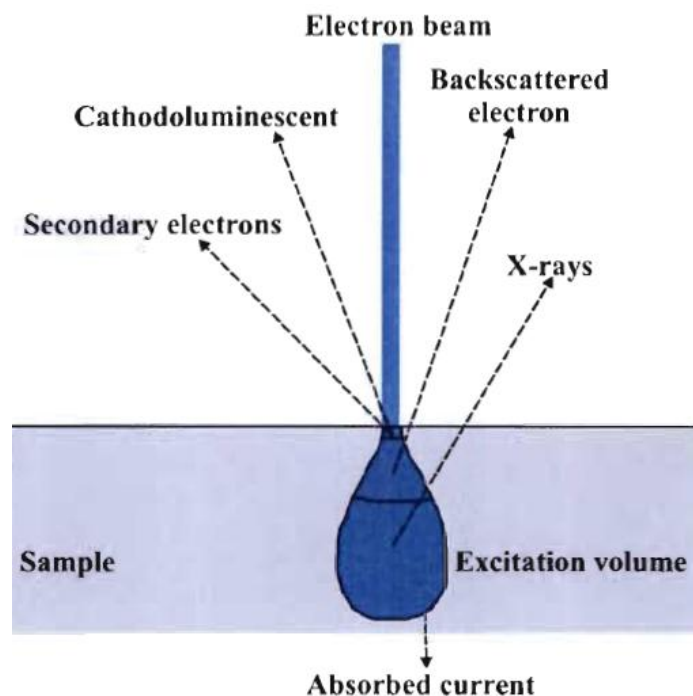


**Figure 2.23** Schematic drawing of signals for a thin sample generated by the impinging electrons [44]

The signals may vary from one location to another as the electron-specimen interaction changes due to, e.g., topography and specimen composition. The magnification of the image is given by the ratio of the length of the scan on the monitor and the corresponding length of the scan on the specimen. For example, an increase in magnification can simply be achieved by decreasing the current of the deflection coils in the microscope column (i.e., lowering the length of the scan on the specimen) and keeping the image size on the monitor constant. It should be mentioned that the magnification also depends on the WD, however, modern SEMs compensate automatically for each WD, thus keeping the displayed magnification correct. Figure 2.23 shows a series of images recorded with increasing magnifications over a range of almost three orders of magnitude.

One of the greatest strengths of the SEM is the tremendous depth of focus, i.e., the range of heights of the specimen being simultaneously in focus (figure 2.24). Due to the small objective aperture diaphragm (about 50-100  $\mu\text{m}$ ) and the large WD the semiangle of the convergent impinging electron probe is in the order of 10 mrad only. At magnifications that are comparable to those of light microscopy (e.g., 1000 $\times$ ) the SEM has a depth of focus that is about 100 times greater than that of an optical microscope, obviously because the semiangle of convergence is much larger in the latter case.

To take full advantage of all the information that SEM can provide, an understanding of its operation modes and the influence of electron beam parameters on the image resolution, the image contrast, the signal strength, and the S/N ratio as well as the electron-specimen interaction is mandatory. The remarkable success of scanning electron microscopy over several decades is mainly due to the tremendous depth of focus, the brilliant image contrast, and the relatively straightforward sample preparation for imaging of surfaces, and, in combination with X-ray microanalytical equipment, its capability of local quantitative element analysis of specimens.

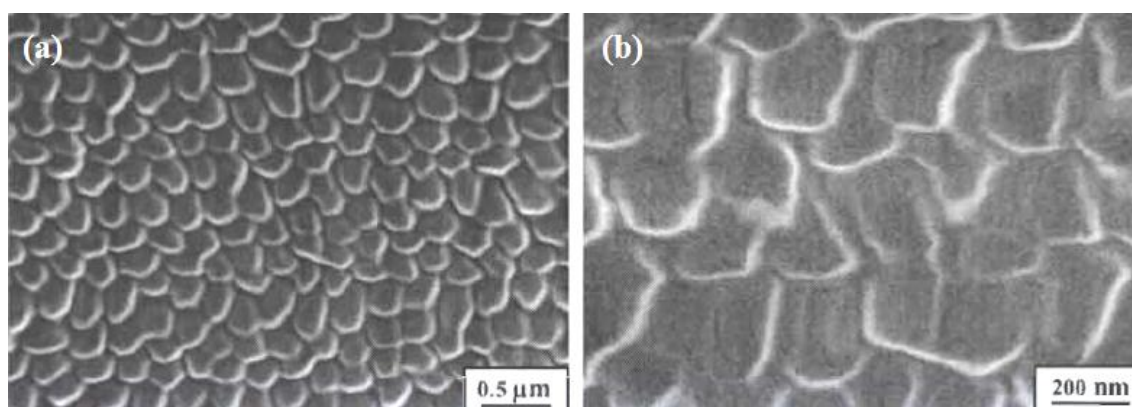


**Figure 2.24** Micrograph of magnification of the head and the eye of a fly, recorded with secondary electrons at 30 kV. The specimen was air dried and sputter coated with about 15 nm gold. The magnification step from (a) to (b) barely reveals further fine of the specimen because of the preparation used. The scale of the micrographs covers about three orders of magnitude [43]

## 2.8 Atomic force microscopy (AFM) [46]



**Figure 2.25** Atomic Force Microscope

Atomic Force Microscope (AFM) provides a 3D profile of the surface on a nanoscale, by measuring forces between a sharp probe ( $<10$  nm) and surface at very short distance (0.2 - 10 nm probe – sample separation). The probe is supported on a flexible cantilever. The AFM tip “gently” touches the surface and records the small force between the probe and the surface. Probes are typically made from  $\text{Si}_3\text{N}_4$ . Different cantilever lengths, materials, and shapes allow for varied spring constants and resonant frequencies as show in figure 2.26. A description of the variety of different probes can be found at various vendor sites. Probes may be coated with other materials for additional SPM applications such as chemical force microscopy (CFM) and magnetic force microscopy (MFM).

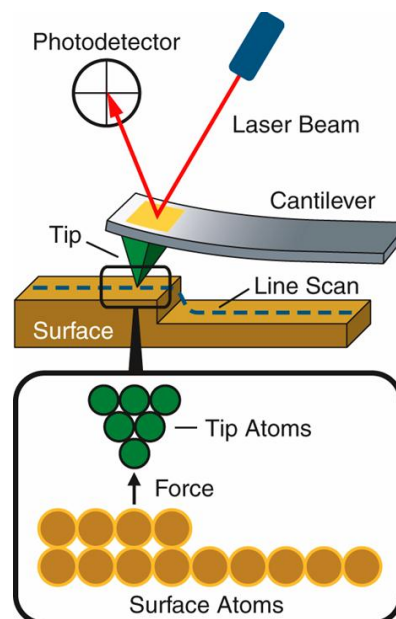


**Figure 2.26** AFM's probe working [46]

There are 3 types of AFM.

### 2.8.1 Contact mode

The cantilever bends, when the spring constant of cantilever is less than surface. The force on the tip is repulsive. By maintaining a constant cantilever deflection (using the feedback loops) the force between the probe and the sample remains constant and an image of the surface is obtained.

- 1.) Advantages: fast scanning, good for rough samples, used in friction analysis
- 2.) Disadvantage: at time forces can damage/ deform soft samples (however image in liquids often resolves this issue)

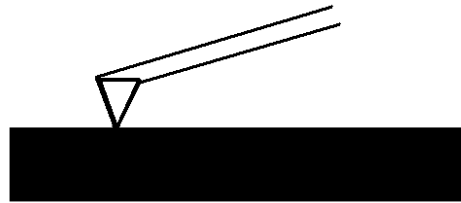


**Figure 2.27** Contact mode

### 2.8.2 Semicontact mode

The imaging is similar to contact. However, in this mode the cantilever is oscillated at its resonant frequency. The probe lightly “taps” on the sample surface during scanning, contacting the surface at the bottom of its swing. By maintaining constant oscillation amplitude a constant tip – sample interaction is maintained and an image of the surface is obtained.

- a. Advantages: allows high resolution of samples that are easily damaged and loosely held to surface; Good for biological samples
- b. Disadvantages: more challenging to image in liquids, slower scan speeds needed

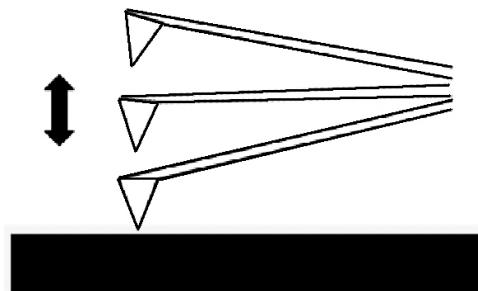


**Figure 2.28** Semicontact mode

### 2.8.3 Non-contact mode

The probe does not contact the sample surface, but oscillates above the adsorbed fluid layer on the surface during scanning. (all samples unless in a controlled UHV or environmental chamber have some liquid adsorbed on the surface). Using a feedback loop to monitor changes in the amplitude due to attractive van der Waals forces the surface topography can be measured.

- a. Advantages: very low force exerted on the sample ( $10^{-2}\text{N}$ ), extended probe lifetime
- b. Disadvantages: generally lower resolution; contaminant layer on surface can interfere with oscillation; usually need ultra-high vacuum to have best imaging.

For thickness analysis, the correcting fluid was used to drop at the corner of the silicon before sputtering. Before characterized by AFM the correcting fluid was removed. Now, AFM can analysis the film thickness.

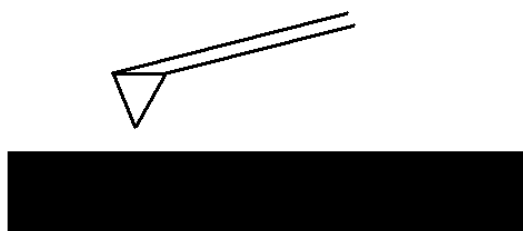


**Figure 2.29** Non-contact mode

## 2.9 Raman spectroscopy [43, 47]

Raman spectroscopy are able to examine microscopic areas of materials by focusing the laser beam down to the micrometer level without much sample preparation as long as a surface of the sample is free from contamination. Raman microscopy (often called micro-Raman), like most Raman spectroscopy, is of the dispersive type. It requires collecting a spectrum in a range of wavenumbers simultaneously. Raman instruments, which consists of the following elements:

- Laser source;
- Sample illumination and collection system;
- Spectral analyzer; and
- Detection and computer control and processing system.

Raman spectroscopy requires highly monochromatic light, which can be provided only by a laser source. The laser source is commonly a continuous-wave laser, not a pulsed laser. The laser source generates laser beams with the wavelengths in the visible light range or close to the range. In a Raman microspectroscopy, sample illumination and collection are accomplished in the microscope. The microscope's optical system enables

us to obtain a Raman spectrum from a microscopic area: this is the main difference between the micro-Raman and conventional Raman spectroscopy. The optical arrangement of a Raman microspectroscopy system is schematically illustrated in figure 2.30. A laser beam passes through a filter to become a single wavelength beam, which is then focused on a sample surface by the microscope. The Raman scattered light reflected from a microscopic area of sample is collected by the microscope and sent to the detector. The Raman scattered light, which results from inelastic scattering, is weak compared with the incident laser light. Thus, a holographic filter has to be used in order to block the laser light entering the detector system. The wavelength of Raman scattering light is selected by a diffraction grating system before being recorded by a detector.

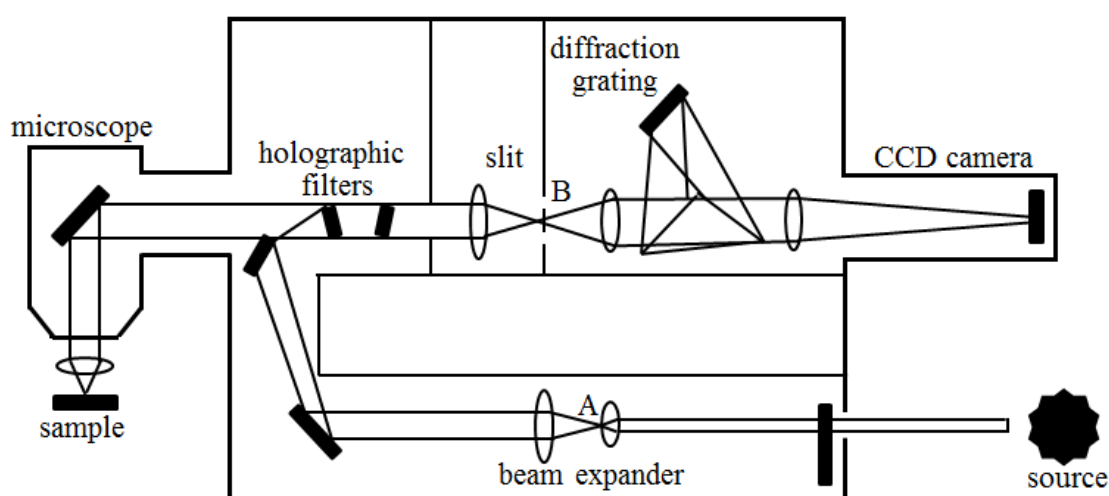


**Figure 2.30** Optical diagram of a Raman spectroscopy [43]

Commonly-used laser sources are gas continuous-wave lasers such as  $\text{Ar}^+$ ,  $\text{Kr}^+$  and He-Ne. Such laser sources are often capable of generating beams of multiple wavelengths. For example,  $\text{Ar}^+$  generates a range of wavelengths with different intensities. The highest intensity wavelengths include 515.4, 488.0 and 350.7 nm. Thus, it is necessary to filter out wavelengths other than 515.4 nm when an  $\text{Ar}^+$  laser is used. The He-Ne laser, however, generates beams of only one wavelength at 632.8 nm. Gas laser sources generate several tens of mW of laser power, but the laser power reaching the microscopic area of the sample is only about 5 mW.

Figure 2.31 showed diagrammatic representation of an energy transfer model of Rayleigh scattering, Stokes Raman and anti-Stokes Raman scattering. The strongest scattering is Rayleigh scatter. In the case of Rayleigh scattering, although there is no resultant change in the energy state of the system, the system still participates directly in the scattering act, causing one photon of incident radiation  $h\nu_0$  to be absorbed and a photon of the same energy to be emitted simultaneously, so that scattering of radiation of unchanged wavenumber,  $\nu_0$ , occurs.

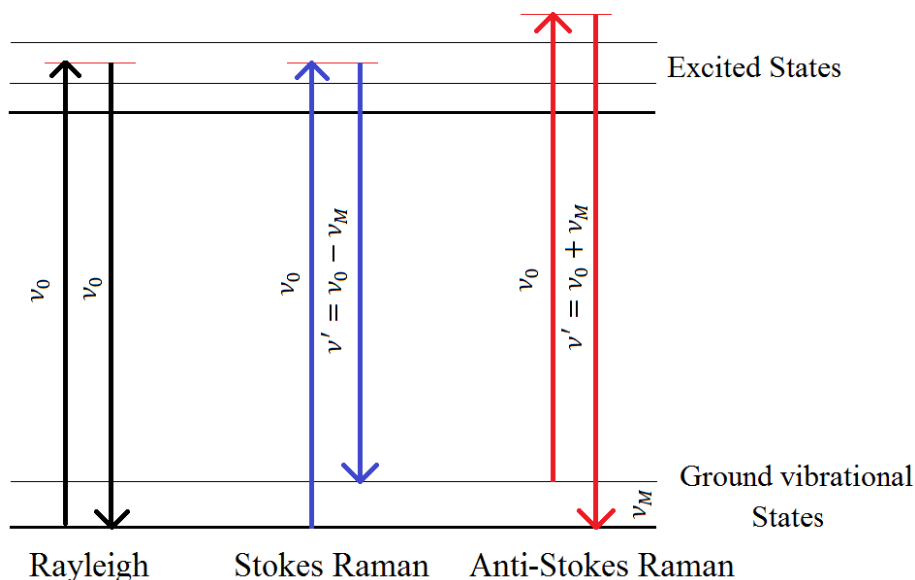


**Figure 2.31** Diagrammatic representation of an energy transfer model of Rayleigh scattering, Stokes Raman and anti-Stokes Raman scattering [47]

It is clear that, as far as wavenumber is concerned, a Raman band is to be characterized not by its absolute wavenumber,  $\nu' = \nu_0 \pm \nu_M$ , but by the magnitude of its wavenumber shift  $\nu_M$  from the incident wavenumber. Such wavenumber shifts are often referred to as Raman wavenumbers. Where it is necessary to distinguish Stokes and anti-Stokes Raman scattering we shall define  $\Delta\nu$  to be positive for Stokes scattering and negative for anti-Stokes scattering, that is  $\Delta\nu = \nu_0 + \nu'$ . Stokes lines are those in which the photon has lost energy to the molecule. Anti-Stokes lines are those in which the photon has gained energy from the molecule.

The intensity of anti-Stokes relative to Stokes Raman scattering decreases rapidly with increase in the wavenumber shift. This is because anti-Stokes Raman scattering involves transitions to a lower energy state from a populated higher energy states.

Stankovich *et al.* [48] shows Raman spectra of reduced graphene oxide (figure 2.32) which obtained from chemical reduction of exfoliated graphite oxide. The Raman spectrum of the reduced graphene oxide also contains both G and D bands (at 1584 and 1352  $\text{cm}^{-1}$ , respectively).

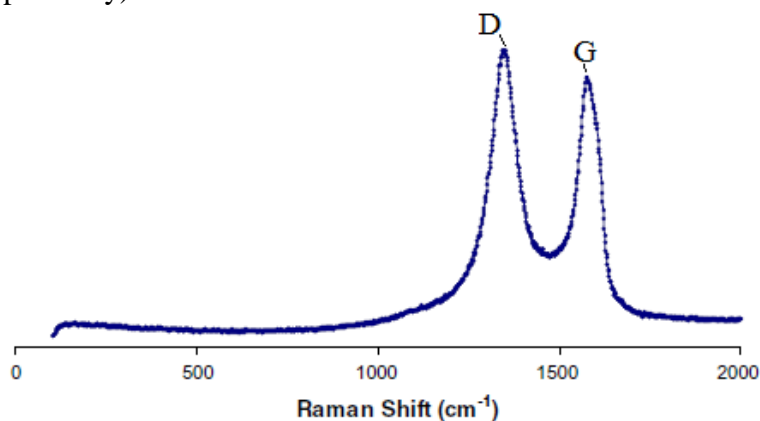


**Figure 2.32** Example of Raman spectra of reduced graphene oxide [48]

## 2.10 Ultraviolet spectroscopy [43, 49]

### 2.10.1. The nature of electron excitation

Most organic molecules and functional groups are transparent in the portions of the electromagnetic spectrum which we call the ultraviolet (UV) and visible (VIS) regions that is, the regions where wavelength from 190 nm to 800 nm. Consequently, absorption spectroscopy is of limited utility in this range of wavelengths. However, in some cases we can derive useful information from these regions of the spectrum.

When continuous radiation passes through transparent materials, a portion of the radiation may be absorbed. If that occurs, the residual radiation, when it is passed through a prism, yields a spectrum with gaps in it, called an absorption spectrum. As a result of energy absorption, atom or molecules pass from a state of low energy (the initial, or ground state) to a state of higher energy (the excited state). Figure 2.33 depicts this excitation process, which is quantized. The electromagnetic radiation that is absorbed has energy exactly equal to the energy difference between the excited and ground state.

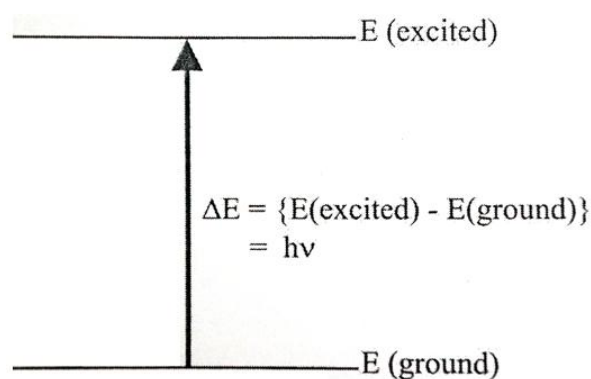


**Figure 2.33** The excitation process;  $E$  = energy of photon (J),  $h$  = Planck's constant ( $6.626 \times 10^{-34}$   $\sigma \cdot s$ ) and  $\nu$  = frequency (Hz) of its associated electromagnetic wave [43]

In the case of ultraviolet and visible spectroscopy, the transition that results in the absorption of electromagnetic radiation in this region of the spectrum are transitions between electronic energy levels. As a molecule absorbs energy, an electron is promoted from an occupied orbital to an unoccupied orbital of greater potential energy. Generally, the most probable transition is from the highest occupied molecular (HOMO) to the lowest unoccupied molecular orbital (LUMO). The energy differences between electronic levels in most molecules vary from 125 to 650 kJ/mole.

For most molecules, the lowest-energy occupied molecular orbitals are the  $\sigma$  bonds. The  $\pi$  orbitals lie at somewhat higher energy levels, and orbitals that hold unshared pairs, the nonbonding ( $\pi$ ) orbitals, lie at even higher energies. The unoccupied, or antibonding orbitals ( $\pi^*$  and  $\sigma^*$ ), are the orbitals of highest energy. Figure 2.34(a) shows a typical progression of electronics energy levels.

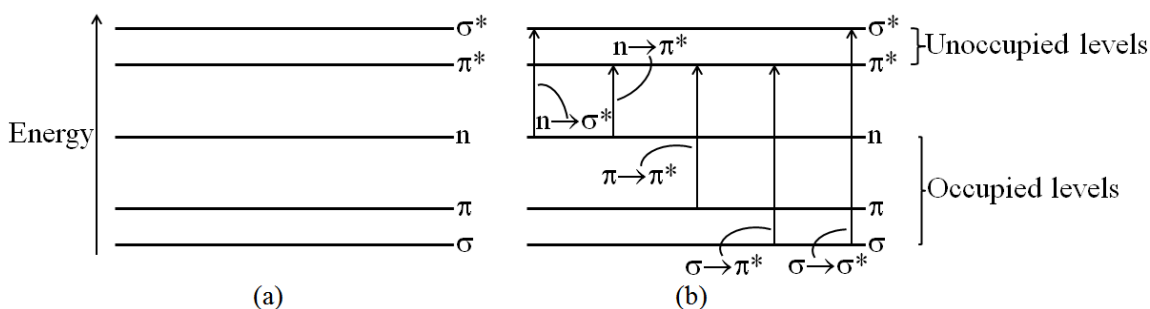


**Figure 2.34** Electronic energy levels and transitions [43]

Clearly, the energy required to bring about transitions from the highest occupied energy level (HOMO) in the ground state to the lowest unoccupied energy level (LUMO) is less than the energy required to bring about a transition from lower occupied energy level. Thus, in figure 2.34(b) an  $n \rightarrow \pi^*$  transition would have a lower energy than a  $\pi \rightarrow \pi^*$  transition. For many purposes, the transition of lowest energy is the most important.

### 2.10.2. The origin of UV band structure

The absorption spectrum sometimes consists of very sharp lines, as would be expected for a quantized process occurring between two discrete energy levels. For molecules, however, the UV absorption usually occurs over a wide range of wavelengths, because molecules (as oppose to atoms) normally have many excited modes of vibration and rotation at room temperature. In fact, the vibration of molecules cannot be completely “frozen out” even at absolute zero. Consequently, a collection of molecules generally has its member in many states of vibration and rotational excitation. The energy level for these state are quite closely spaced, corresponding to energy difference considerably smaller than those of electronic level. The rotational and vibrational levels are thus “superimposed” on the electronic levels. A molecule may therefore undergo electronic and vibrational-rotational excitation simultaneously, as shown in figure 2.35.

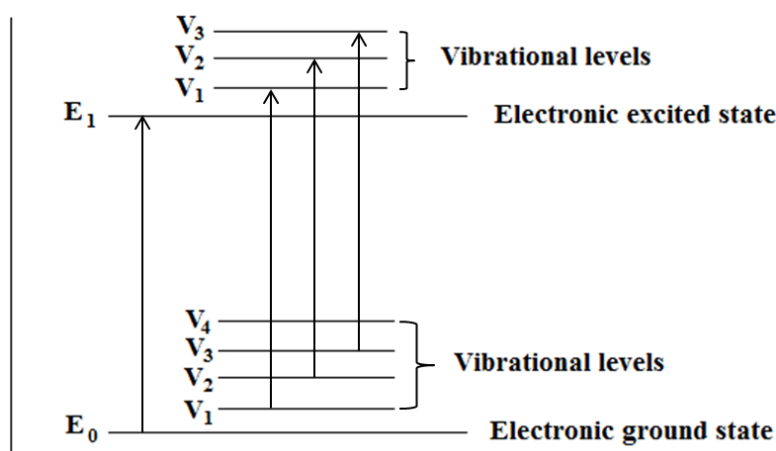


**Figure 2.35** Electronic transitions with vibrational transitions superimposed. (Rotational levels, which are very closely spaced within the vibrational levels, are omitted for clarity) [43]

Because there are so many possible transitions, each differing from the others by only a slight amount, each electronic transition consists of a vast number of lines spaced so closely that the spectrophotometer cannot resolve them. Rather, the instrument traces an “envelope” over the entire pattern. What is observed from these types of combined transitions is that the UV spectrum of a molecule usually consists of a broad band of absorption centered near the wavelength of the major transition.

### 2.10.3. Principles of absorption spectroscopy

The greater the number of molecules is capable of absorbing light of a given wavelength, the greater the extent of light absorption. Furthermore, the more effectively a molecule absorbs light of a given wavelength, the greater the extent of light absorption. From these guiding ideas, the following empirical expression, known as the Beer-Lambert law, may be formulated.

$$A = \log(I/I_0) = \epsilon cl \quad (2.1)$$

$A$  = absorbance  
 $I_0$  = intensity of light incident upon sample cell  
 $I$  = intensity of light leaving sample cell  
 $C$  = molar concentration of solute  
 $l$  = length of sample cell (cm)  
 $\epsilon$  = molar absorptivity ( $L \text{ mol}^{-1} \text{ cm}^{-1}$ )

The term  $\log(I/I_0)$  is also known as the absorbance (or the optical density) and may be represented by  $A$ . The molar absorptivity (formerly known as the molar extinction coefficient) is a property of the molecule undergoing an electronic transition and is not a function of the variable parameters involved in preparing a solution. The size of the absorbing system and the probability that the electronic transition will take place control the absorptivity, which ranges from 0 to  $10^6$ . Values above  $10^4$  are termed high-intensity absorption, while values below  $10^3$  are low-intensity absorptions.

Many compounds absorb UV or visible light. Figure 2.36 showed a beam of monochromatic radiation of radiant power  $P_0$ , directed at a sample solution. Absorption takes place and the beam of radiation leaving the sample has radiant power  $P$ .

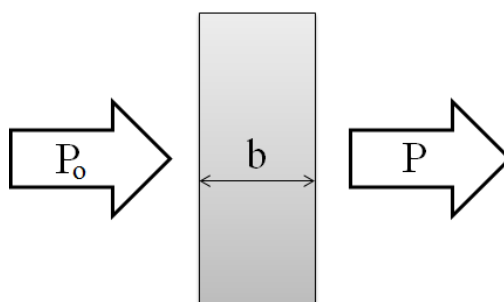


**Figure 2.36** A beam of monochromatic radiation of radiant power  $P_0$ , directed at a sample solution. Absorption takes place and the beam of radiation leaving the sample has radiant power  $P$ .

The amount of radiation absorbed may be measured in a number of ways:

$$\text{Transmittance, } T = P/P_0 \quad (2.2)$$

$$\% \text{ Transmittance, } \%T = 100T \quad (2.3)$$

$$\text{Absorbance, } A = \log_{10} P_0/P \quad (2.4)$$

$$A = \log_{10} 1/T \quad (2.5)$$

$$A = \log_{10} 100/\%T \quad (2.6)$$

$$A = 2 - \log_{10} \%T \quad (2.7)$$

Equation 2.7 is worth remembering because it allows you to easily calculate absorbance from percentage transmittance data.

Paredes *et al.* [21] showed UV-vis absorption spectra of as-prepared graphite oxide dispersed in different solvents by means of bath ultrasonication as shown in figure 2.37. The spectra are plotted in the wavelength range from 200 to 1000 nm. Water displays the best dispersing ability because it provides the highest absorption intensity and therefore the largest amount of suspended graphite oxide, followed closely by DMF and NMP. Ethylene glycol and THF exhibit very similar dispersing abilities toward as-prepared graphite oxide, although they are noticeably smaller than water, DMF and NMP. Moreover, as-prepared graphite oxide cannot disperse in ethanol because it does not provide the absorption intensity.

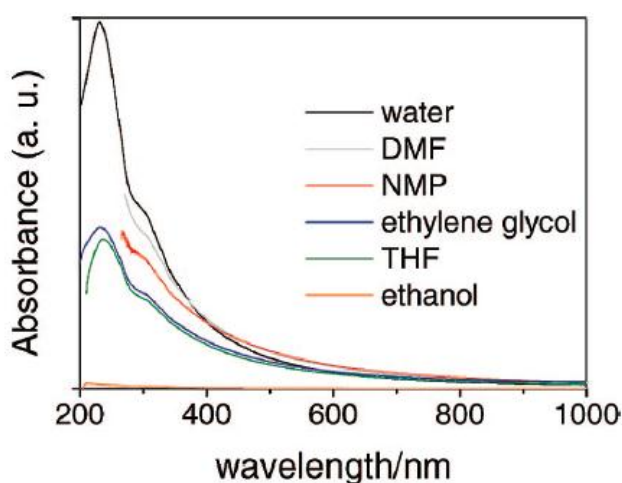


**Figure 2.37** Example of UV-vis absorption spectra of as-prepared graphite oxide dispersed in different solvents by means of bath ultrasonication [21]

## 2.11 Transmission electron microscopy (TEM) [50]

Transmission electron microscopy (TEM) is a technique whereby a beam of electrons is transmitted through an ultrathin specimen, interacting with the specimen as it passes through. An image is formed from the interaction of the electrons transmitted through the specimen. The image is magnified and focused onto an imaging device or screen.

TEM has magnification and resolution capabilities that are over a thousand times beyond that offered by the light microscope. It is an instrument that is capable of

revealing ultrastructure and magnified images of a thin specimen, typically with a magnification in the range  $10^3$  to  $10^6$ .

TEM is electron analogue of the optical compound microscope. The sample is illuminated uniformly with electrons which pass through it to form an image. The ultimate resolution of this instrument is determined by the wavelength of the electron and the numerical aperture of lens, as described above.

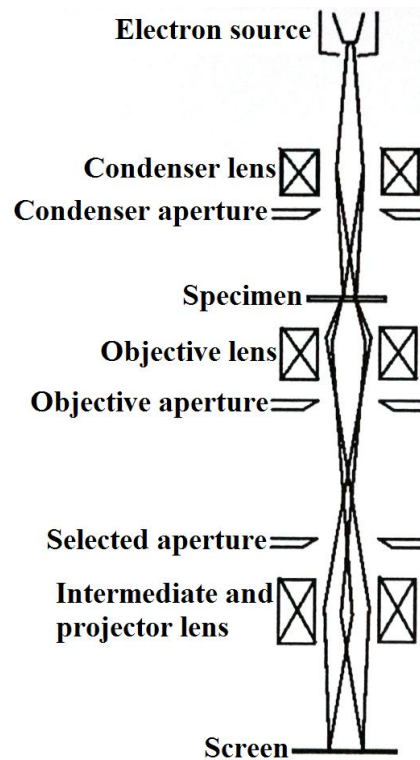


**Figure 2.38** Schematic diagram of transmission electron microscope [51]

A schematic diagram of TEM is shown in figure 2.38. The source of electrons is a heated tungsten filament. This is biased to about 100 keV, which accelerates the electrons through the condenser lens on to the specimen. The condenser aperture restricts the size of the beam to reduce unnecessary illumination of the specimen, since electron beams do damage materials to some extent. The sample itself is very thin (around 100 nm) so that most of the electrons pass through it without significant inelastic scattering. Complex thinning procedures are often necessary for semiconductors, using chemical thinning or ion beam milling. Vibrations in the atomic composition or thickness of the sample produce changes in the electron scattering from the main beam. In addition, if the sample is crystalline, strong Bragg diffraction of the electron beam will occur in specific directions, forming sharp spots in the back focal plane of the objective lens. As with the optical microscope, the unscattered beam may be accepted into the image, contrast being obtained when features in the solid scatter electrons out of the beam so that they do not continue along the microscope (bright field imaging). If the contrast thereby obtained is small, then only the scattered electrons are collected (dark field imaging). The scattered electrons are collected by the objective

lens forming a diffraction pattern of the object in the back focal plane of the lens and an intermediate image of the object in the image plane of the objective. The objective lens is the critical component for the microscope. As can be seen from the diagram, it is only lens for which the electrons have a large angle to the axis. It will therefore be a major contribution of aberration in the system.

The objective aperture provides contrast by selecting or intercepting scattered or unscattered electrons so that bright field or dark field imaging can be achieved. The intermediate and projector lenses magnify the image produced by the objective lens before projecting it on to a screen. These lenses do not contribute significantly to aberration since the angle the electron beam makes to their axes is small.

The TEM can be used to study the crystallographic structure of solids. This is accommodated by the intermediate lens. The focal length of a magnetic lens can be changed easily by changing its electric current. The focal length of the intermediate lens can be adjusted so that, instead of the image plane, the back focal plane of the objective lens is imaged at the object plane of the projector lens. The electron diffraction pattern of the crystalline solid occurs at the back focal plane of the objective lens, and it is this which is now amplified and projected on to the viewing screen. This image will contain information on the crystallographic structure of the solid. By employing a selected area aperture, the area of the specimen contributing to the diffraction pattern may be limited. The diffraction patterns obtained depend on the crystallographic orientation of the semiconductor.

Defects present in the semiconductor also give characteristic diffraction pattern features which can be used to characterize them. Images of such defects in crystals can be produced by utilizing the local changes in the Bragg scattering they produce due to local distortions in the crystal planes. A diffraction beam can be selected (or blocked) by the objective aperture and monitored. The changes in Bragg scattering in the region of the defect will then produce contrast in the transmitted electron beam.

The diffracted beams may also be used to produce what are known as lattice images. To produce these, the undeflected beam and one of the deflected beams are allowed to reach the image plane. Since they have travelled different path lengths, they will interfere, producing fringes which represent the planes of the atoms in the solid. The angle of deflection of a diffracted beam will depend on the lattice plane spacing.

Antisari et al. [24] showed TEM image of graphite milled for 20 hour as shown in figure 2.39. The presence of thin and relatively wide lamellae can be observed. Several features related to the crystal structure of the particle can be noticed, as can be seen in the blow-up (inset in the figure 2.38). Each lamella show different set of lattice fringes at the border and in the inner part, respectively. The set of fringes at the border has the spacing of the (002) lattice planes so that their number can be a measurement of the thickness of the single lamella.

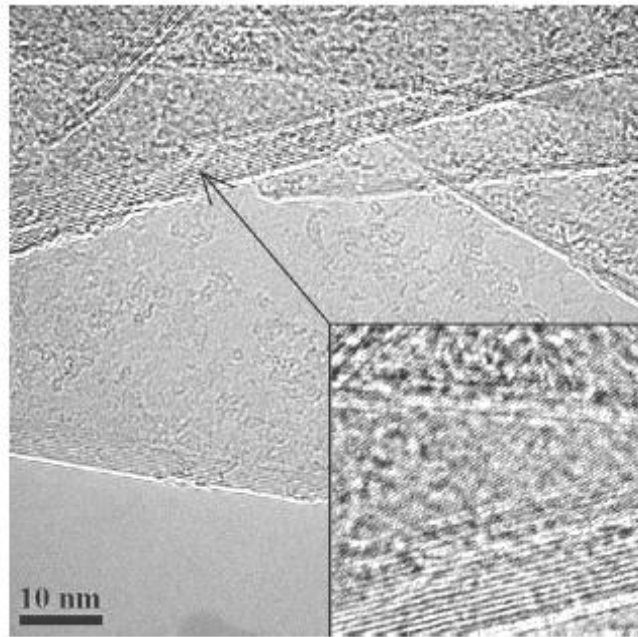


**Figure 2.39** Example of TEM image of graphite milled for 20 hour [24]

## 2.12 Sputtering deposition [52, 53]



**Figure 2.40** Sputtering deposition

Sputtering is a physical vapor deposition (PVD) process where material is physically removed from a target by energetic ion bombardment. The word “sputtering” comes from the Dutch “sputteren” which mean “to spit out in small particles and with a characteristic explosive sound”. Sputtering was first observed by Groves in 1852 with Plücker first to suggest, in 1858, that this discovery be used as a tool to produce metallic films. Groves initially called the phenomena “cathodic disintegration”, and it was renamed “sputtering” by Sir John Thompson in 1921. In 1923 Thompson dropped the “l” and the term “sputtering” has lasted to this day.

Sputtering is referred to a physical process as it is simply a momentum exchange between particles with no chemical reactions occurring. Early plasma processing found removal of material from the cathode to be an inconvenience, as the destruction of the cathode would result. Sputtering is a powerful tool used for the deposition of thin film, in chemical analysis, etching and cleaning. Sputtering is commonly utilized for thin film deposition, as the extremes for melting or chemically reacting high melting point materials are not required, as with evaporation or an electrochemical process.

Target is the surface of the solid. The sputtering mechanism can be explained by an ion approaches the target. There are five interactions of ions with surfaces as shown in figure 2.41. One or all of the following phenomena may occur.

1. The ion may be reflected, probably being neutralized in the process. This reflection is the basis of an analytical technique known as Ion Scattering Spectroscopy, which enables us to characterize the surface layers of the material, and also tell us a lot of about the fundamental ion-surface interaction.
2. The impact of the ion may cause the target to eject an electron, usually referred to as a secondary electron.
3. The ion may become buried in the target. This is the phenomenon of ion implantation, which is already used extensively in integrate circuit technology for selectivity doping silicon wafer with precisely controlled amounts and depth profiles of specific impurities, and is likely to find many other applications such as surfaces treatment of steels.
4. The ion impact may also be responsible for some structural rearrangements in the target material. Rearrangements may vary from simple vacancies (missing atoms) and interstitials (atoms out of position) to more gross lattice defected such as changes of stoichiometry (i.e. relative proportions) in alloy or compound targets, or to charge levels and distribution, and are usually collectively referred to as radiation damage, which is a subject of great importance, particularly with relation to nuclear energy. Radiation damage can often be removed by annealing (heat treatment) but it is not always unwanted, and perhaps the alternative name or altered surface layer, used mostly to describe the stoichiometry changes, is more apt.
5. The ion impact may set up a series of collisions between atoms of target, possibly leading to the ejection one of these atoms. This ejection process is known as sputtering.

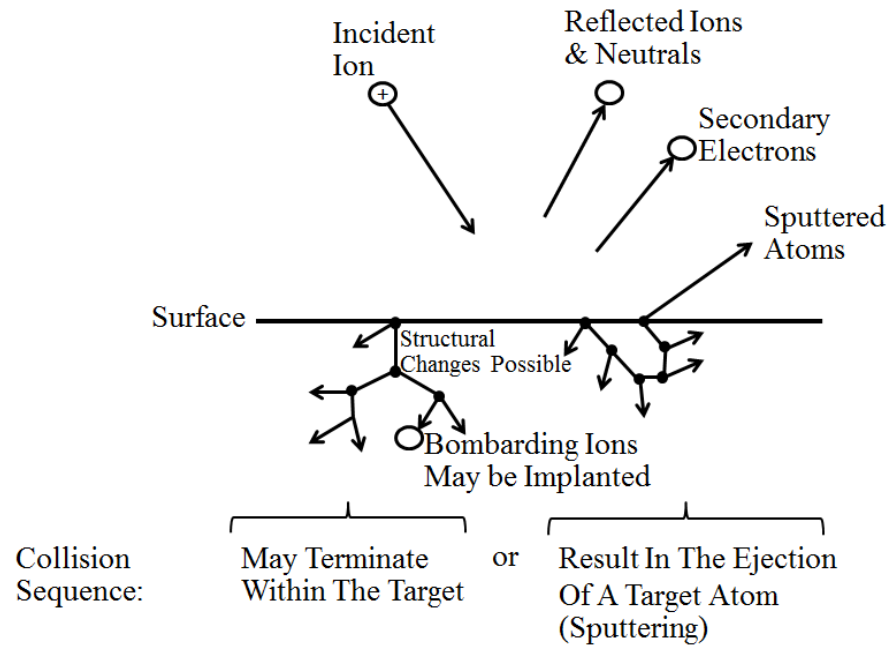


**Figure 2.41** The interactions of ions with surfaces [53]